A&A 440, 623–636 (2005)
DOI: 10.1051/0004-6361:20052668

Astronomy & Astrophysics

Diffusive convective overshoot in core He-burning intermediate mass stars

I. The LMC metallicity

P. Ventura[1], M. Castellani[1], and C. W. Straka[2]

[1] Osservatorio Astronomico di Roma, Via Frascati 33, 00040 Monte Porzio Catone, Italy
e-mail: [ventura; m.castellani]@mporzio.astro.it
[2] Department of Astronomy, Yale University, PO Box 208101, New Haven, CT 06520-8101, USA
e-mail: straka@astro.yale.edu

Received 11 January 2005 / Accepted 8 May 2005

Abstract. We present detailed evolutionary calculations focused on the evolution of intermediate mass stars with 3 $M_{\odot} \leq M \leq$ 9 $M_{\odot}$ of metallicity typical of the Large Magellanic Cloud (LMC), i.e. $Z = 0.008$. We carefully compare the models calculated by adopting a diffusive scheme for chemical mixing, in which nuclear burning and mixing are self-consistently coupled, while the eddy velocities beyond the formal convective core boundary are treated to decay exponentially, and those calculated with the traditional instantaneous mixing approximation. We find that: i) the physical and chemical behaviour of the models during the H-burning phase is independent of the scheme used for the treatment of mixing inside the CNO burning core; ii) the duration of the He-burning phase relative to the MS phase is systematically longer in the diffusive models, due to a slower redistribution of helium to the core from the outer layers; iii) the fraction of time spent in the blue part of the clump, compared to the stay in the red, is larger in the diffusive models. The differences described in points ii) and iii) tend to vanish for $M > 6$ $M_{\odot}$. In terms of the theoretical interpretation of an open cluster stellar population, the differences introduced by the use of a self-consistent scheme for mixing in the core with adjacent exponential decay are relevant for ages in the range 80 Myr $< t <$ 200 Myr. These results are robust, since they are insensitive to the choice of the free-parameters regulating the extension of the extra-mixing region.

Key words. stars: evolution – stars: interiors – stars: Hertzprung Russell (HR) and C-M diagrams

1. Introduction

The stars of intermediate mass (hereinafter IMS) are by definition those massive enough to undergo helium burning, but that never reach conditions in the central regions leading to ^{12}C ignition: soon after the end of helium burning in the core they undergo a phase of thermal pulses, during which the star for most of the time is supported energetically by a CNO burning shell, with periodic and thermally unstable ignition of 3α reactions in a stellar layer above the CO core (Schwarzschild & Harm 1965, 1967; Iben 1975, 1976); eventually, mass loss determines a general cooling of the structure and later evolution as a CO white dwarf.

During the last decades the interest in the evolution of this class of objects has increased, because they were suggested to be the responsible for the chemical anomalies observed at the surface of globular cluster stars (Gratton et al. 2004): the idea behind this hypothesis is that an early generation of IMS evolved on short time-scales within the cluster, and polluted the interstellar medium with nuclearly processed material, so that a new generation of stars formed in an environment which, from a chemical point of view, might show the anticorrelations currently observed (Cottrell & Da Costa 1981; D'Antona et al. 1983; Ventura et al. 2001, 2002).

During the two phases of nuclear burning in the central regions, the IMS develop extended convective cores, the sizes of which increase with mass. On the theoretical side the duration of these phases, and the path followed by the tracks in the HR diagram, are uncertain because of the unknown behaviour of the convective eddies as they approach the formal border of the core, the location of which is found via the traditional Schwarzschild criterion. Unfortunately, this latter criterion allows us to locate the point where buoyancy vanishes, but the distance (due to inertia) convective eddies travel beyond the border cannot be inferred.

Traditionally, in the evolution codes, this extra-mixing region, which is formally radiative, has been simulated by assuming that the zone out of the formally convective core which is fully homogenised has a geometrical width which is parametrised as $\alpha H_{\rm p}^{\rm b}$, where $H_{\rm p}^{\rm b}$ is the pressure scale height at

the border of the core, and α is a free parameter that is calibrated to reproduce the MS of open clusters (instantaneous mixing). Detailed comparisons of theoretical predictions with photometric studies of open clusters have shown that a value of $\alpha \approx 0.2$ is needed for IMS, at least for $M > 2\ M_{\odot}$ (see e.g. Maeder & Meynet 1991; Stothers & Chin 1992).

Alternatively, the extra-mixing beyond the formal convective border may be simulated by assuming that the velocities of the convective eddies decay exponentially, with a more physical description, in which mixing of chemicals and nuclear burning are self-consistently coupled (diffusive scheme) (Deng et al. 1996a,b; Herwig et al. 1997; Ventura et al. 1998).

In a recent paper focused on reproducing the stellar population of the clump region of the LMC cluster NGC 1866, Ventura & Castellani (2005, hereinafter VC05) showed that using a diffusive approach within the convective core of the IMS leads to a longer stay of the evolutionary tracks in the blue part of the HR diagram during the He-burning phases; this, in turn, helped in reconciling the observed scenario for NGC 1866 (in which the ratio B/R between stars burning helium in the blue and red region of the clump is $\approx$1) (Testa et al. 1999) with the theoretical predictions (a $B/R \approx 0.8$ is found with the diffusive case, to be compared to $B/R \approx 0.4$ if an instantaneous scheme is adopted). The particular scheme adopted to deal with chemical mixing inside the He-burning convective core turned out to be by far the most relevant physical input influencing the distribution of stars in the clump region of the HR diagram, when compared to other model uncertainties of, e.g., the assumptions made upon the extension of the extra-mixing region, the cross sections used for the $^{12}C+\alpha$ reaction, and the convective model adopted to find out the temperature gradient within regions unstable to convection. A further important result of that study was that the whole He-burning phase was longer in the diffusive models, so that larger t_{He}/t_{H} ratios are expected.

The conclusions of the afore-mentioned paper might hold in principle just for the range of masses relevant for the study of the clump region of NGC 1866 (i.e. $\approx$ 4–4.5 $M_{\odot}$); the idea behind this paper is therefore to extend the above analysis to a wider range of masses, ranging from the minimum mass undergoing an overall contraction during the core He-burning phase leading to a meaningful excursion of the track to the blue (i.e. 3 $M_{\odot}$) through the whole range of IMS stars. We decided to extend our analysis further, up to 9 $M_{\odot}$. We postpone to a forthcoming paper a wider analysis, including the effects of metallicity.

We carefully compare the results obtained with the instantaneous and the diffusive scheme for chemical mixing for all the masses involved. We also test for the correct distribution of stars which should be expected in the clump region of the HR diagram at different ages (hence, mass in the clump). Our aim is to understand in which cases (hence, for which masses and ages) the use of a diffusive scheme to deal with nuclear burning and chemical mixing within the He-burning cores of IMS is mandatory for a reliable estimate of the relative duration of the various evolutionary phases.

We provide a description of the main physical inputs of the code used to calculate the evolutionary sequences in Sect. 2. In Sect. 3 we present and discuss the main properties and the various evolutionary phases of the diffusive models, focusing in particular on the He-burning phase; we evaluate the reliability of our results for the description of the kinematic behaviour of the convective eddies in the proximity of the border of the core, comparing the velocities found via the use of the local FST convective scheme with those obtained with a more physically sound non-local treatment. Finally, we discuss the differences between the diffusive models and those calculated with the instantaneous mixing approximation in Sect. 4, where we also suggest the range of masses and ages for which the use of the diffusive approach is recommended.

2. The stellar evolution code

All the evolutions presented and discussed in this paper were calculated by means of the code ATON2.1, a full description of which can be found in Ventura et al. (1998), with the last updates given in Ventura & D'Antona (2005); the interested reader may find in the two above papers all the details concerning the numerical structure of the code, and the micro- and macro-physics input.

Here we want just to recall some of the physical inputs most relevant for this work:

- The temperature gradient within instability regions can be found either by the traditional Mixing Length Theory (MLT, Böhm-Vitense 1958; Vitense 1953), or via the Full Spectrum of Turbulence (FST) model (Canuto & Mazzitelli 1991).
- Within regions unstable to convective motion, it is possible to deal with nuclear burning either by assuming that mixing is instantaneous (so that the whole convective region is assumed to be always chemically homogenised), or by simultaneously treating nuclear burning and mixing of chemicals; in this latter case we solve for each of the nuclear species included in the network the diffusion equation (Cloutman & Eoll 1976):

$$\left(\frac{\mathrm{d}X_i}{\mathrm{d}t}\right) = \left(\frac{\partial X_i}{\partial t}\right)_{\mathrm{nucl}} + \frac{\partial}{\partial m_{\mathrm{r}}}\left[(4\pi r^2\rho)^2 D \frac{\partial X_i}{\partial m_{\mathrm{r}}}\right] \quad (1)$$

stating mass conservation of element i. The diffusion coefficient D is taken as

$$D = \frac{1}{3} v l \quad (2)$$

where v is the convective velocity and l is the convective scale length.

Within this diffusive framework it is necessary to specify how convective velocities decay outside the convective boundaries (Deng at al. 1996a,b; Herwig et al. 1997; Ventura et al. 1998). In agreement with Xiong (1985) and Grossman (1996) and supported by the numerical simulations by Freytag et al. (1996), we assume that convective velocities decay exponentially outside the formal convective boundary as:

$$v = v_{\mathrm{b}} \exp \pm \left(\frac{1}{\zeta f_{\mathrm{thick}}} \ln \frac{P}{P_{\mathrm{b}}}\right) \quad (3)$$

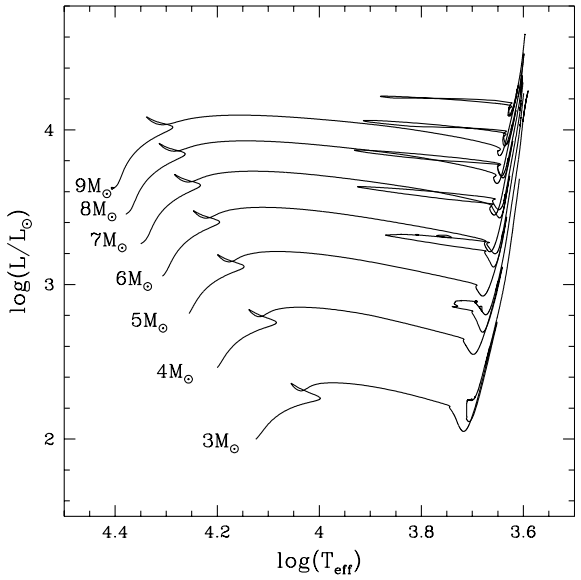

Fig. 1. Stellar tracks on the HR diagram related to the evolution of the intermediate mass diffusive models. Labels indicate the stellar mass. The pre-MS evolution was omitted for clarity reasons.

where v_b and P_b are, respectively, turbulent velocity and pressure at the convective boundary, P is the local pressure, ζ a free parameter connected with the e-folding distance of the decay, and f_{thick} is the thickness of the convective regions in fractions of H_p.

In the instantaneous case the geometrical width of the extra-mixing region is parametrised as $l_{ov} = \alpha H_p$. The physical meanings of the parameters ζ (diffusive models) and α (instantaneous) are strongly different (see the detailed discussion above this argument in VC05), but, in terms of the duration and extension of the MS phase, we find that $\alpha = 0.2$ is equivalent to $\zeta = 0.03$. These are the values of α and ζ which will be used for our analysis.

– All the nuclear cross-sections are taken from Angulo et al. (1999), with the only exception of the $^{12}C(\alpha,\gamma)^{16}O$ reaction, for which we employ the more accurate determination by Kunz et al. (2002).

3. The evolution of the diffusive models

The diffusive models were calculated by adopting a chemical composition typical of the LMC, i.e. $Z = 0.008$ and $Y = 0.25$ (Brocato et al. 2003; Barmina et al. 2002). For all the other elements we assumed solar-scaled abundances.

Convection was treated according to the FST framework: we recall, however, that one of the main results of VC05 was that the convective model influences only the colour and the slope of the giant branch in the HR diagram, but not the thermodynamic structure of the convective cores (both during hydrogen and helium burning), or the duration of the different evolutionary phases.

In agreement with VC05, we used the diffusive scheme to couple nuclear burning and chemical mixing; the coefficient ζ for the exponential decay of velocities out of the convective cores was set to $\zeta = 0.03$. No extra mixing from the base of the convective envelope was considered.

Breathing pulses were suppressed, by preventing any growth of the convective core once the central abundance of helium drops below 0.05.

Figure 1 shows the tracks followed by the models considered on the theoretical plane $\log(T_{eff}) - \log(L/L_\odot)$. The evolutions were calculated starting from the early evolutionary stages, but the pre-MS phase was omitted for clarity.

The main properties of the IMS models are reported in Table 1.

Table 1. Physical properties of the diffusive models.

M_{ZAMS}	$t(H)^a$	$M^b_{core,H}$	$M^d_{1std.up}$	$\log\left(\frac{L_{tip}}{L_\odot}\right)$	$M^c_{core,He}$	$t(He)^a$	t^a_{red}	t^a_{blue}
3.0	363	0.63	0.53	2.75	0.20	75	75	0
4.0	179	0.97	0.84	3.11	0.30	25	16	9
5.0	106	1.29	1.18	3.43	0.42	13	8	4
6.0	72	1.64	1.52	3.70	0.56	7.3	5.3	2
7.0	52	2.00	1.89	3.93	0.72	4.9	3.6	1.3
8.0	40	2.38	2.29	4.12	0.92	3.6	2.6	0.9
9.0	32	2.81	2.71	4.29	1.17	2.9	2.2	0.6

[a] Times are expressed in Myr.
[b] Maximum extension (in solar masses) of the convective core during H-burning.
[c] Maximum extension (in solar masses) of the convective core during He-burning.
[d] Mass coordinate (in solar masses) of the innermost layer reached during the first dredge-up.

During the MS phase all models attain temperatures in the central regions sufficiently high to convert protons to helium via the CNO cycle; this in turn favours the formation of a convective core. As can be seen in the 3rd column of Table 1, the maximum extension (in mass) of the core is an increasing function of the total mass, ranging from 0.63 $M_\odot$ for the 3 $M_\odot$ model to 2.81 $M_\odot$ for $M = 9$ $M_\odot$. The duration of the whole phase of hydrogen burning (t_H) decreases with mass: we find $t_H = 363$ Myr for $M = 3$ $M_\odot$, down to $t_H = 32$ Myr for $M = 9$ $M_\odot$.

As can be seen from Fig. 1 the stars, soon after central hydrogen exhaustion, undergo a phase of general expansion of the outer layers, while CNO burning continues within a shell lying above the contracting core (Iben 1993). The decrease of the effective temperature favours the inwards penetration of the convective envelope, which reaches layers previously touched (at least partially) by CNO burning, in what is commonly known as the first dredge-up episode. Column 6 of Table 1 reports the mass coordinate of the innermost layer reached by the external convection during this process: we see that the mass of the whole external envelope at the maximum penetration of the surface convection increases with mass, reaching a maximum value of $\delta M \approx 8$ $M_\odot$ for the 9 $M_\odot$ model.

As the CNO shell moves outwards the luminosity increases, until the temperature in the centre reaches values sufficiently high to favour helium burning via the 3α reactions. We see that

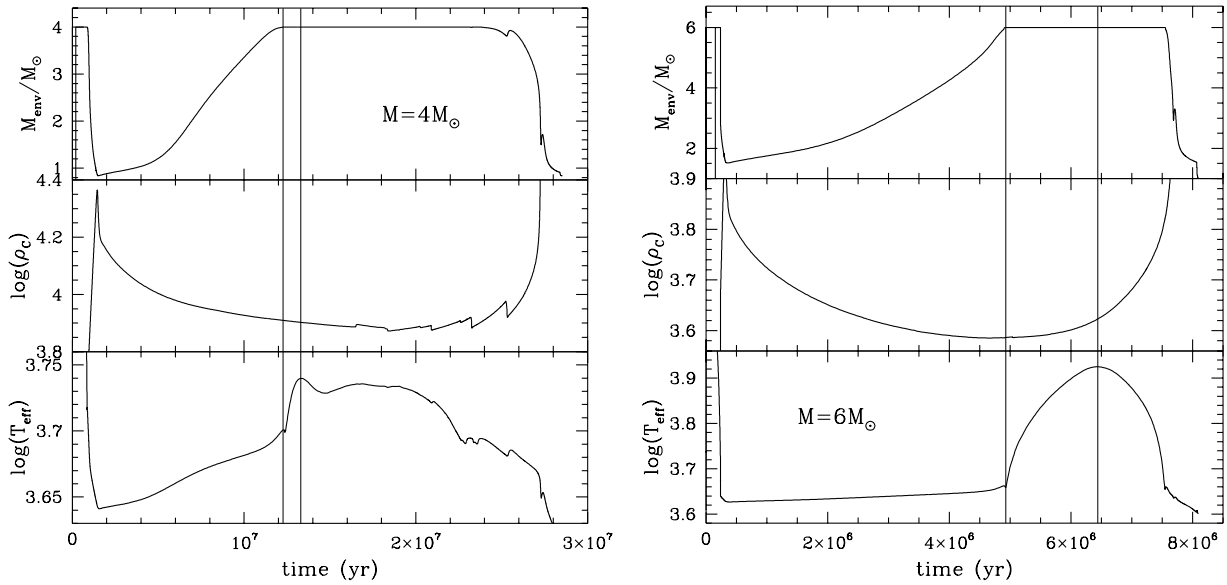

Fig. 2. The temporal evolution of some physical quantities related to the evolution of two stellar models of mass 4 $M_\odot$ (*left*) and 6 $M_\odot$ (*right*). For each mass the variation with time of the base of the convective envelope (*top*), central density (*middle*) and effective temperature (*bottom*) is reported. The thin vertical lines in both panels indicate the time when the surface convection is extinguished (which is coincident with the beginning of the excursion of the track to the blue) and when the bluest point on the HR diagram is reached.

the temperature at which helium burning begins is slightly dependent on mass, ranging from $T_c \approx 120{\times}10^6$ K for $M = 3\ M_\odot$ to $T_c \approx 148 \times 10^6$ K for $M = 9\ M_\odot$. The beginning of core He-burning is accompanied by an expansion of the central regions, with the subsequent cooling of the CNO shell, so that the stellar luminosity reaches a tip value (reported for each model in Col. 5 of Table 1) and then decreases.

All the main steps related to the evolution of IMS through the helium burning phase, and the occurrence of the blue loops on the HR diagram, are well documented in the literature (see e.g. Chiosi et al. 1992), and will not be repeated here. We only want to recall the main factors triggering the excursion of the tracks towards the blue and the relative duration of the stay in this region (VC05):

- The overall contraction leading to the bluewards excursion starts as soon as the surface convection disappears.
- The tracks stay in the blue until the scarcity of helium in the central regions forces the core to contract, with the consequent expansion of the external layers.
- The duration of the blue phase is therefore connected with the helium still left in the core when the blue region of the clump is reached: the lower the helium mass fraction, the shorter is the stay in the blue.

A rapid glance at Cols. 8 and 9 of Table 1 shows that the percentage of time spent in the blue compared to the red is decreasing with mass, ranging from $t_{\rm blue}/t_{\rm red} \approx 0.7$ for the 4 $M_\odot$ model to $t_{\rm blue}/t_{\rm red} \approx 0.25$ for $M = 9\ M_\odot$. We also note from Fig. 1 that the extension of the loops decreases for $M > 7\ M_\odot$.

The decrease with mass of the fraction of the total He-burning time spent in the blue can be understood by looking at Fig. 2, where we report the temporal evolution of the He-burning phase of two models with masses $M = 4\ M_\odot$ (left) and $M = 6\ M_\odot$ (right) in terms of the variations with time of the base of the convective envelope ($M_{\rm env}$), central density ($\rho_{\rm C}$), and effective temperature ($T_{\rm eff}$).

We see that the excursion to the blue, which can be identified by a rapid change of slope of the variation with time of $T_{\rm eff}$, starts as soon as the surface convection is extinguished. As can be seen by comparing the left and right top panels, the mass of the envelope at the beginning of the He-burning phase is larger for the more massive models, so that by the time that the surface convection vanishes the helium left in the centre is lower: the consequence is that for larger masses, as soon as the track reaches the bluest point, the contraction of the core, which can be seen by the increase of the central density shown in the middle panels of Fig. 2, follows shortly afterwards, hence the track returns quickly to the red. If we compare the evolution of the central densities of the two models, we see that in the 4 $M_\odot$ model the central regions are still expanding when the maximum $T_{\rm eff}$ is reached, while in the 6 $M_\odot$ model the core has just started contracting.

Even the shorter extension of the loops of the largest masses which can be seen in Fig. 1 can be explained on the basis of the percentage of helium in the core when the surface convection disappears. In Fig. 3 we show the details of the evolution of the 8 $M_\odot$ model, during the core He-burning phase. In this case we also show the variation of the central helium (right-bottom panel). The vertical thin lines mark, respectively, the stage when the overall contraction begins, and when the bluest point of the track in the HR diagram is reached. We see that when the surface envelope disappears the helium left in the core is less than 40%, and more important, when the bluest point is reached $Y_{\rm C} \approx 0.1$, and the core contraction has already begun (see the right-top panel). In this case, therefore, the scarcity of helium triggers the core contraction while the track was still moving to the blue, with a consequent shorter extension of the loop.

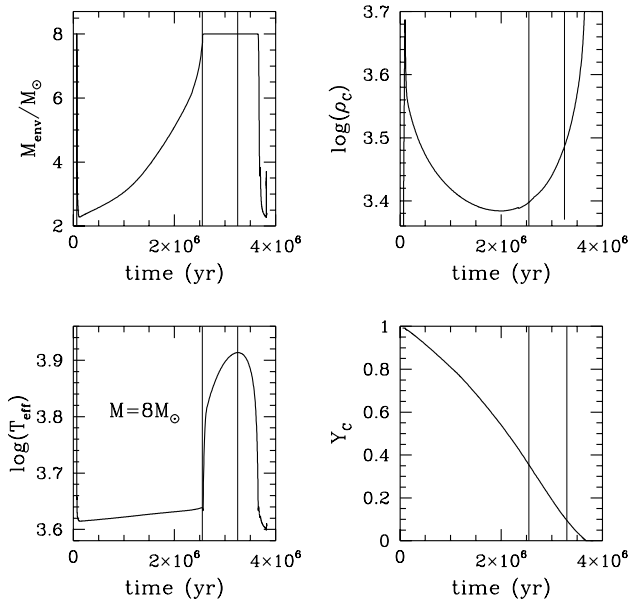

Fig. 3. The variation with time of some physical and chemical quantities of the evolution of a 8 $M_{\odot}$ diffusive model: we show the mass of the base of the surface convection (*top-left panel*), the central density (*top-right*), the effective temperature (*bottom-left*) and the central mass fraction of helium (*bottom-right*). The thin vertical lines have the same meaning as in Fig. 2.

3.1. Semiconvection

Figure 1 (and in more details also the left panel of Fig. 4) shows that the tracks of the lowest masses of our sample are characterised by some loops of minor extension on the HR diagram; this happens only after the bluest point is reached, when the helium abundance dropped to values $Y_{\rm C} \leq 0.2$. The high mass tracks do not show such irregularities.

As expected, we could verify that the occurrence of such loops, with a temporary increase of both luminosity and effective temperature, is connected with a sudden increase of the helium mass fraction in the whole core, with the consequent rapid increase of the helium burning rate in the central regions. Traces of these episodes can also be seen in the temporal variation of the central density of the 4 $M_{\odot}$ model reported in Fig. 2 (left-middle panel). These irregularities are due to the formation of a small convective region in the proximity of the border of the convective core, triggered by the appearance of a minimum in the profile of the radiative logarithmic temperature gradient $\nabla_{\rm rad}$ (Castellani et al. 1971a,b, 1985; Alongi et al. 1993). We verified that any change in the temporal or spatial resolution used in calculating the evolutions may only shift sligthly the location of these loops in the HR diagram, but cannot prevent these irregularities, because the small convective shell is formed in any case.

We went into the details of the evolution of the 4 $M_{\odot}$ model, which is the typical mass showing such irregular behaviour. Figure 4 shows the path followed by the model in the HR diagram focused on the clump region (solid track, left panel), and the evolution of the thermodynamic structure of the core in the $\log(\rho) - \log(T)$ plane at some selected evolutionary stages (right panel), corresponding to some fixed values of the central helium abundance, and marked by full dots in the left panel. We note that while the core temperatures increase for the whole helium burning phase, the densities first decrease and then begin to increase when $Y_{\rm C} < 0.3$.

The two panels of Fig. 5 show the internal variation of opacity (left panel) and radiative gradient (right) for the same 6 models shown in Fig. 4. In the region of the $\log(\rho) - \log(T)$ plane covered by the core of the 4 $M_{\odot}$ model, i.e. $3.4 < \log(\rho) < 4$ and $7.9 < \log(T) < 8.2$ (see the right panel of Fig. 4) we know that the dominant contribution to the opacity is provided by Thompson scattering, but with a non negligible contribution by free-free transitions. This latter term shows a "thermodynamic" dependence of the form $\rho/T^{3.5}$ (which explains the increase of the opacity when moving from the centre of the star outwards) and a chemical factor which increases for larger ^{12}C and ^{16}O abundances (Castellani et al. 1985). The two above terms, for a given mass shell, tend to balance each other, because as He-burning proceeds the temperature increases and the helium mass fraction decreases, so that the two contributions show an opposite behaviour: this is the reason why for each value of the internal mass the value of κ inside the core is approximately constant. The situation for the border of the mixed region, where we have a drop of the helium abundance and a maximum of the opacity, is different, because its temperature is almost constant as the evolution proceeds: this maximum value of the opacity is therefore growing (see the left panel of Fig. 5). It is this growing contribution of the opacity which eventually leads to the formation of a local maximum of the radiative gradient, as can be seen in the right panel of Fig. 5.

From the above discussion it is clear that a fundamental condition for the appearance of the local maximum of the opacity is that the stellar layers must be helium poor: this makes this question relevant only in the final part of this evolutionary phase, when the helium content in the central layers drops to $Y_{\rm C} < 0.2$. This is confirmed by the smoothness of the solid track of Fig. 4 in the early phases of He-burning.

Numerically, in a diffusive framework, the treatment of the convective zone close to the central core is not straightforward, because any exponential decay from a convective region so thin in mass is highly unreliable: we might decide in this case to stick to the Schwarzschild criterion, and to ignore any overshooting, but this choice is confirmed to trigger the afore-mentioned discontinuities when this small instability region vanishes.

To eliminate these irregularities we decided, in the case when the convective shell is very close to the central core, to ignore its presence for what concerns the calculation of the velocity profile, i.e. to assume the same velocity field (and particularly the same exponential decay from the core) which we would have if all the stellar layers external to the core were radiatively stable.

The result is the dotted track in the left panel of Fig. 4, which is much more smooth than the corresponding solid line. We also verified that the global time of helium burning, as well as the relative duration of the blue and red phases of the clump, are practically identical in the two cases, because any sudden increase of the helium abundance in the central regions has the

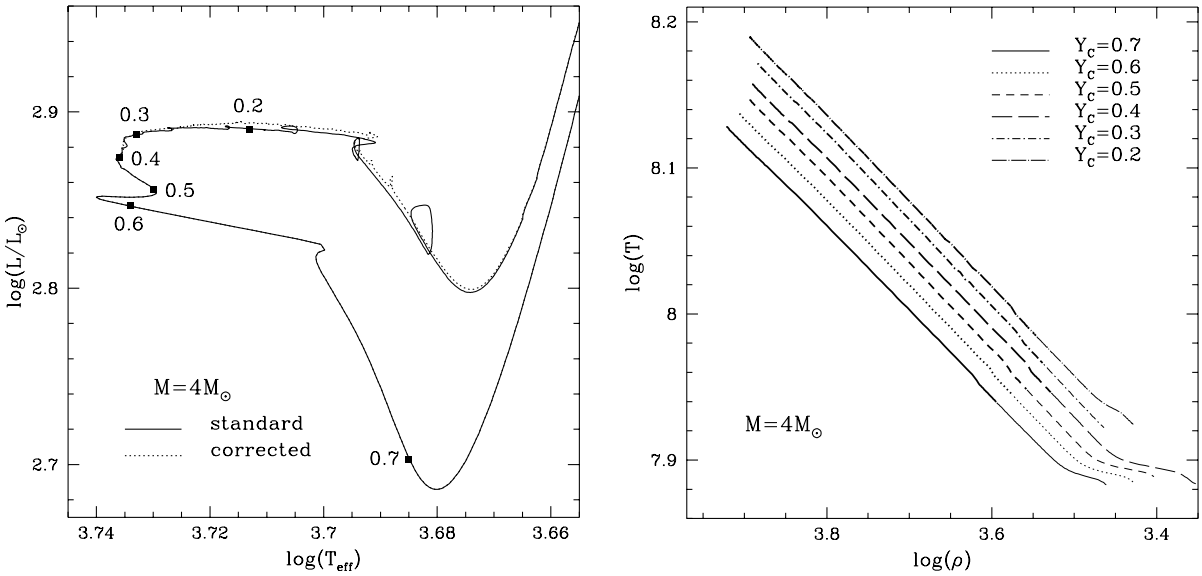

Fig. 4. *Left*: the path followed in the HR diagram of a 4 $M_\odot$ diffusive model during the He-burning phase (solid line); the labels on the track indicate the corresponding values of the central helium mass fraction. The dotted line corresponds to a model where any convection zone in the proximity of the core was ignored in the calculation of the velocity profile following the method described in the text. *Right*: the internal structure of the He-burning core of the same 4 $M_\odot$ model reported on the left panel in the $\log(\rho) - \log(T)$ plane. The structures refer to the evolutionary stages marked with square dots on the track in the left panel. The thick parts refer to the zone which is formally convective according to the Schwarzschild criterion.

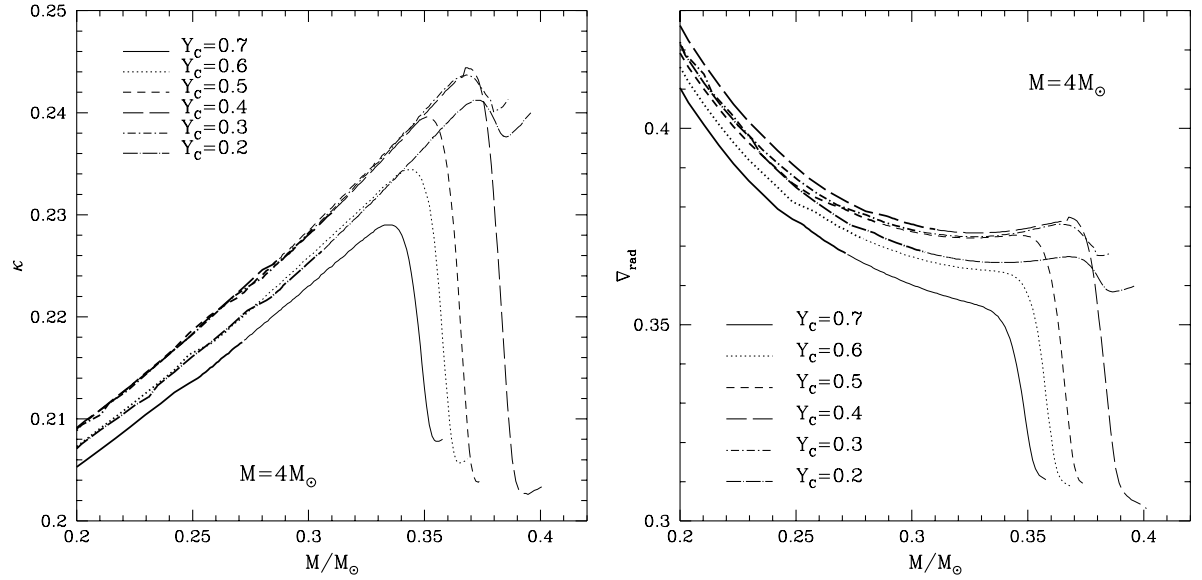

Fig. 5. The internal distribution of opacity (*left panel*) and radiative temperature gradient (*right*) within the core of a 4 $M_\odot$ model at the same evolutionary stages of Fig. 4. We see that the increase of the opacity coefficient at the border of the core leads eventually to the formation of a local minimum of $\nabla_{\rm rad}$.

effect of increasing the reaction rates of the helium burning reactions, and this compensates the larger mass fraction of helium, which would lead to a larger He-burning time.

To understand why these sudden increases of the central helium mass fraction are not found in the evolution of the more massive models, we show in Fig. 6 the internal structure of the core of the 8 $M_\odot$ model at various evolutionary stages identified by some fixed values of the central mass fraction of helium, in the $\log(\rho) - \log(T)$ plane (left panel) and in terms of the opacity profile (right panel). If we compare the right panel of Fig. 4 with the left panel of Fig. 6 we see that the core of the 8 $M_\odot$ model occupies a region in the $\log(\rho) - \log(T)$ plane which is approximately at the same temperature as the 4 $M_\odot$ model, but at lower densities: in this region the deviation of the opacity coefficient from the Thompson value are expected to be lower, and this is confirmed by the right panel of Fig. 6, where we can see that the the values of κ within the core are within $0.15 < \kappa < 0.19$, to be compared to the much wider range observed in the left-panel of Fig. 5 (in making the comparison between the two figures, note that in the 4 $M_\odot$ case only the outer part of the core is reported, while in Fig. 6 the whole central region is shown).

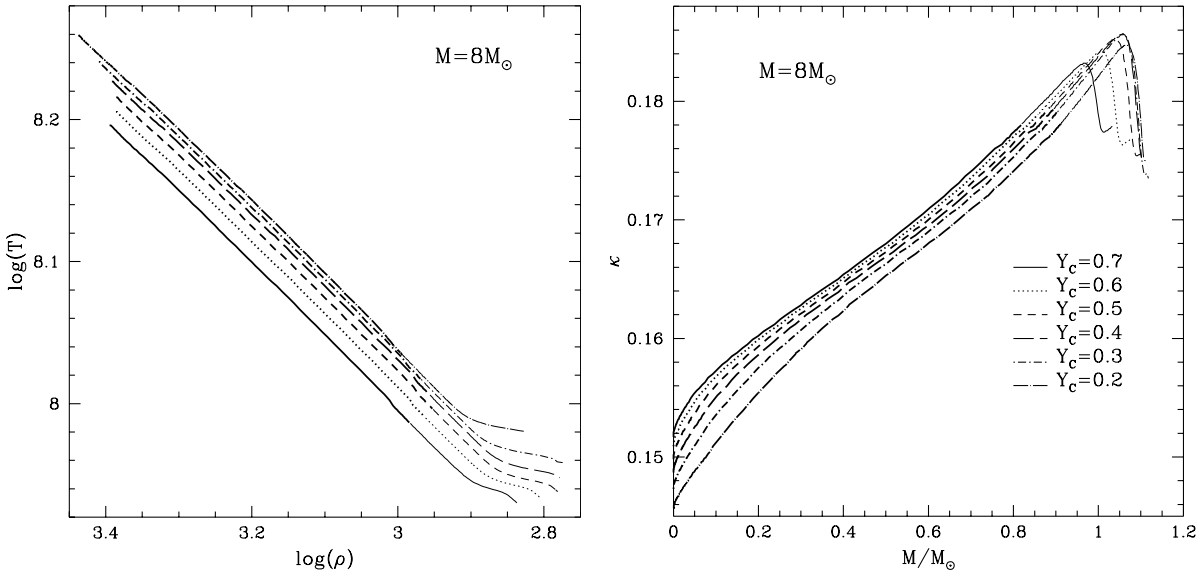

Fig. 6. The structure of the core of a 8 $M_{\odot}$ model during the He-burning phase at various evolutionary stages corresponding to some fixed values of the central mass fraction of helium. *Left*: the $\log(\rho) - \log(T)$ plane. *Right*: the opacity coefficient.

The maximum values of the opacity coefficient found at the border of the convective core ($M \approx 1\ M_{\odot}$) of the 8 $M_{\odot}$ model are therefore too low to cause the formation of a local maximum in the $\nabla_{\rm rad}$ profile, so that no convective zones in the proximity of the core are found.

3.2. The velocity field

As we saw at the beginning of this section, the rapidity with which helium is consumed within the core plays a fundamental role in determining the time which IMS spend in the blue region of the clump in the HR diagram. We will see in the following section that the time-scale of the core He-burning phase is the main difference between the diffusive models and those calculated with the instantaneous mixing approximation: these latter models, burning helium more rapidly, stay very shortly in the blue.

Within the diffusive framework, nuclear burning and mixing are coupled via Eq. (1). The diffusive coefficient D is found via Eq. (2), and is dependent on the mean velocity of the convective eddies, v. A reliable estimate of v is therefore mandatory in determining correctly the importance of the diffusive term relatively to the nuclear rates. Wrong values of the velocities, particularly in the regions next to the border of the core, might lead to an incorrect extension of the region beyond the Schwarzschild border which is fully homogenised, and, even more important for our purposes, of the zone external to the core where we still have some mixing, though on times comparable to those typical of nuclear burning in the interiors.

In the FST context of turbulent convection, the velocity is found by means of Eq. (88) in Canuto et al. (1996): we recall that in the FST model the whole spectrum of eddies is taken into account, starting from the largest scales, of dimensions comparable to the length of the whole convective zone, to those typical of the molecular dissipation processes.

The FST model is local, in the sense that the convective gradient is calculated exclusively on the basis of physical quantities taken at the same locus where we calculate the gradient itself: this, unfortunately, neglects one of the essential features of the Navier-Stokes equations, i.e. non locality. We therefore may wonder how the velocities found in the FST context of convection depend on the assumptions which are at the basis of the model itself.

We therefore decided to compare our velocities with those found by adopting a non-local theory, developed by Kuhfuß (1986). Kuhfuß derives an equation for the specific turbulent kinetic energy by proper spherically averaging the first order perturbed Navier-Stokes equations. The approach is similar to the models by, e.g., Xiong (1981), Stellingwerf (1982, 1984) and Canuto (1997), and it shares with them the principal difficulty of modelling the unknown correlation functions of the fluctuating quantities. In the Kuhfuß model this is done within the framework of anelastic and diffusion type approximations thereby introducing free parameters for every term arising in the equation. Altogether we are left with five free parameters. Kuhfuß fixes two of them by matching the convective velocity and the convective flux with the corresponding MLT values and we use the same values here. The remaining parameters consist of a mixing length parameter, which we set close to the solar value of 1.6 and an overshooting parameter. The latter regulates the terms governing the non-locality and it is the most relevant parameter for the velocities at the Schwarzschild boundary and the subsequent penetration of convective eddies beyond this formal boundary.

Although we do not claim to have employed a final theory of convection, the one from Kuhfuß is an improvement over MLT since it allows predictions of time-dependency and non-locality based on the hydrodynamic equations. It is worth noting that in the stationary, strictly local limit a cubic equation similar to MLT is retained when the Ledoux criterion is employed. In addition, the Kuhfuß theory gives the same

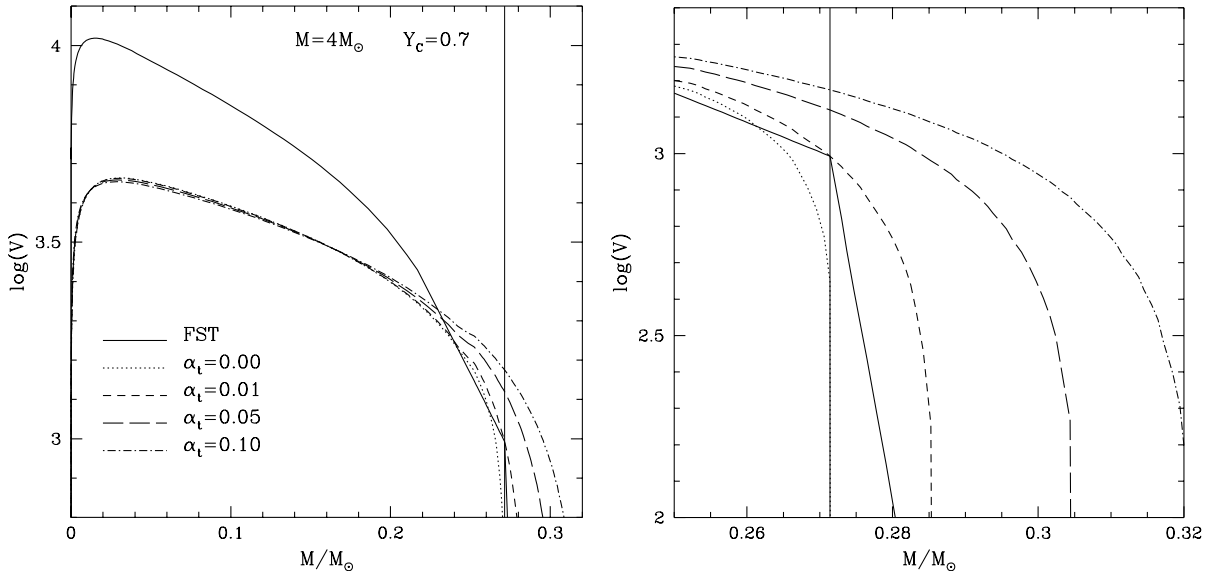

Fig. 7. Convective velocities inside the core of a 4 $M_\odot$ model during the phase of core He-burning, when the central helium mass fraction is $Y_C = 0.7$. In the left panel we report the whole convective core, in the right we focus in the regions close to the formal border, indicated by the thin vertical line. The solid line corresponds to the FST, the remaining to the Kuhfuß case for four different overshoot parameters in the range $\alpha_t = 0$–0.10.

qualitative behaviour for the temperature stratification in the overshooting region as derived by Zahn (1991). In the following, stationary solutions of the Kuhfuß equation are calculated and compared with the FST treatment.

We focus our attention on the same evolutionary stages shown in Fig. 4, and perform a detailed comparison between the internal profile of the velocity provided by the FST treatment with the values predicted by the Kuhfuß theory for the same thermodynamic stratification. We stress here that our goal is neither to give a definite answer on how the convective eddies move in the convective core, nor which is their behaviour at the formal border; this is far beyond the scope of the present paper. Our main goal is simply to test the robustness of the velocities we use inside the inner parts of the convective core up to the formal boundary, comparing the results obtained by two completely different approaches. Before going into the details of such a comparison, we are essentially interested in stellar regions close to the formal border of the core fixed by the Schwarzschild criterion for the following reasons:

1. In the deep interiors of the core, as we will also show in the following section, the rapidity of the convective motions is so high compared to the nuclear processes that it is possible to assume that from a chemical point of view these regions are completely homogenised.
2. In the proximity of the border the time scale of convection increases, and the transport of chemicals becomes slower.
3. In the framework of extended convection with exponential decay for the convective velocities, as expressed in Eqs. (3), a key-role is played by the velocity v_b at the border of the core itself: here, it is this quantity that eventually determines the extension of the region beyond the formal border where we find some chemical mixing.

Figure 7 shows the velocity profiles inside the convective core of a 4 $M_\odot$ model, when the central mass fraction of helium is $Y_C = 0.7$. We focus on this mass because we will see that it is the model where the differences between the diffusive and the instantaneous schemes are most pronounced.

In the left panel we report the whole convective core, while in the right panel we show only the regions close to the border. The solid line indicates the velocities found through the FST model, while the other lines refer to velocities calculated by the Kuhfuß theory, each corresponding to a different value of the overshooting parameter α_t. As can be seen in the right panel, velocities in the model with $\alpha_t = 0$, which corresponds to strictly local convection, terminate exactly at the Schwarzschild boundary. Any overshooting is regulated by switching on the non-local terms, i.e. $\alpha_t > 0$. The exact value of α_t is highly uncertain, therefore we have chosen to calculate a few models with $\alpha_t = \{0.005, 0.01, 0.05, 0.10, 0.20\}$. The right panel of Fig. 7 shows that the best match of the velocity at the formal boundary between Kuhfuß model and FST corresponds to a model with $\alpha_t = 0.01$ which is equivalent to small overshooting of $0.06 H_p^b$. This is slightly smaller than would be expected on other grounds, since the best estimate for the overshooting distance derived from isochrone fitting to colour-magnitude diagrams of open clusters, e.g., by Prather & Demarque (1974), Maeder & Mermilliod (1981), Pols et al. (1998) and Demarque et al. (1994) yield a canonical value of $0.23 H_p^b$ which would correspond to $\alpha_t \approx 0.15$. In any case, the velocities at the boundary deviate at most by a factor of 1.6 which can be regarded as a close match considering that the velocities are derived by completely different approaches.

In the deep interior we see a qualitatively similar behaviour, with a maximum value which is reached $\approx 0.02\ M_\odot$ away from the centre: we note that there is a difference of a factor of ≈ 2

between the peak values, the FST model giving $v_{\rm max} \approx 110$ m s^{-1}, to be compared to $v_{\rm max} \approx 55$ m s^{-1} provided by the Kuhfuß modelling.

In the proximity of the border, the two models provide essentially the same result, i.e. $v_{\rm b} \approx 10$–15 m s^{-1}, and this holds practically for all the Kuhfuß models, independently of the overshooting parameter. From the right panel of Fig. 7, we see that the values of the velocities found via the FST scheme plus the assumed exponential decay are comparable to those provided by the Kuhfuß models, with the closest match found for small overshooting parameters.

We could verify that the similarity of the results concerning the profile of velocity close to the formal border of the core during the He-burning phase still holds, qualitatively and quantitatively, until $Y_{\rm C} > 0.4$. At later evolutionary stages the problems discussed in this section make the results obtained extremely sensitive to the way in which the small convective zone which develops away from the core is treated, and how it is related to the core itself. In this case a comparison between the local and the non-local model is not straightforward, because the results provided by the latter turn out to be much more strongly dependent than the previous phases on the overshooting parameter: for the same thermodynamic stratification, we may have either two distinct separated convective zones, or the formation of a unique central instability region, which, given the high values of the velocity ($v_{\rm min} \approx 6$ m s^{-1}), will be fully homogenised.

The results in this case are much more uncertain. Yet, we are mainly interested in the relative duration of the blue phase of the core He-burning, which is determined by the rapidity with which helium is consumed in the core before the bluest point of the track is reached: therefore, our main interest is to evaluate the robustness of the estimates of the velocities close to the formal border of the convective core during earlier phases, when $Y_{\rm C} \geq 0.5$.

We therefore find that in the models with masses $M \approx 4\ M_{\odot}$, which we will see to be those for which the results obtained depend critically on the adopted scheme for mixing, the values of the velocity found via the FST model in the regions close to the border of the core for the evolutionary phases preliminary to the bluest point of the track are within a factor of 1.5 consistent with those found by using a completely different approach, in which convection is treated non locally: though we do not claim to have solved the problem of understanding how the convective eddies are slowed down by the opposition of the buoyancy forces, we are confident that our estimate is not far from the true value, which gives robustness to our results.

4. The comparison between diffusive and instantaneous models

In most of the modern evolutionary codes, with only a few exceptions (see e.g. Stancliffe et al. 2004), mixing of chemicals inside the regions unstable to convection is treated as it was instantaneous, i.e. the time scale of convection is assumed to be much shorter than the time scales of all the reactions included in the network, so that it is assumed that the whole convective region is instantaneously homogenised: this assumption allows us to deal simultaneously with nuclear burning and mixing,

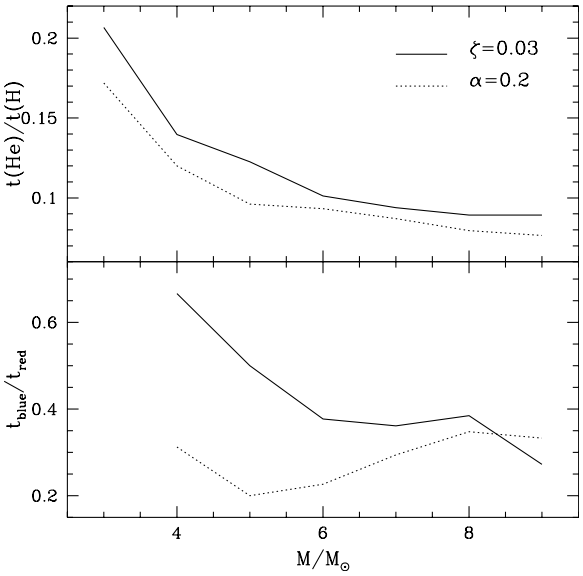

Fig. 8. *Top*: the comparison of the ratio of the He-burning and the H-burning times for various masses between the diffusive (solid line) and the instantaneous models (dotted). *Bottom*: the comparison of the ratio between the time spent in the blue and in the red region of the clump during the He-burning phase for stellar models of different mass calculate with the diffusive (solid) and the instantaneous (dotted) scheme for mixing.

so that the whole instability zone is treated as if it was a single mesh-point, for which average cross-sections and chemical abundances are found and used.

On purely theoretical grounds the two processes should be considered simultaneously, and the above simplification could be used and is expected to give results in agreement with the self-consistent treatment only if all the relevant nuclear reactions everywhere inside the convective region are much slower than the process of mixing; we stress here that in order to have similar results the above condition must hold also in any extra-mixing region, i.e. in any region beyond the formal border fixed by the Schwarzschild criterion where it is assumed that some sort of mixing happens, despite the opposition of buoyancy.

We calculated two sets of models, which were evolved from the pre-MS phase up to the beginning of the AGB:

1. The diffusive models presented and discussed in the previous section, with a parameter for the exponential decay of velocity $\zeta = 0.03$.
2. A set of models in which the mixing of the chemical elements within the convective core and in the extra-mixing region is assumed to be instantaneous. In this case we used an overshooting distance of $0.2H_{\rm p}$: this choice is motivated by the fact that this overshooting distance leads to results very similar to those of the diffusive models with $\zeta = 0.03$ in terms of the extension and the duration of the main sequence of the single stars (VC05).

Figure 8 shows for the two sets of models and for each mass the ratio of the helium burning time compared to the MS time (top panel) and the ratio between the times spent, respectively, in the blue and in the red part of the HR diagram during the helium burning phase (bottom panel).

The top panel of Fig. 8 shows that the He-burning time, relatively to the H-burning time, is systematically lower in the instantaneous models. From the bottom panel we can see that the difference between the diffusive and the instantaneous models in terms of $t_{\rm blue}/t_{\rm red}$ ratio decreases with mass, and eventually vanishes for $M \approx 8\ M_{\odot}$.

The different amount of helium still present in the central core when the overall contraction begins (i.e. when the surface convection is extinguished) is the reason of the longer stay of the diffusive models in the blue region of the clump, with respect to the instantaneous models. In the 4 $M_{\odot}$ model the central helium mass fractions when the excursion of the track to the blue begins are $Y_{\rm C} \approx 0.65$ and $Y_{\rm C} \approx 0.40$, respectively, for the diffusive and the instantaneous model. For the largest masses, this difference decreases, and eventually vanishes for $M = 8\ M_{\odot}$, for which we find $Y_{\rm C} \approx 0.30$ in both cases: this explains why the solid and the dotted lines cross in the bottom panel of Fig. 8.

Before entering into the details of the models, we also note from the same panel that $t_{\rm blue}/t_{\rm red}$ reaches a minimum value for $M \approx 7\ M_{\odot}$ for the diffusive models and $M \approx 5\ M_{\odot}$ for the instantaneous set, and is almost constant for higher masses. The occurrence of the minimum marks approximately the border between the models for which the surface convection is extinguished when the core is still expanding ($Y_{\rm C} > 0.4$) and those for which the helium mass fraction at the beginning of the excursion towards the blue part of the HR diagram is so low that the central regions are beginning to contract to satisfy the stellar energy demand: in the instantaneous case the minimum is reached for a lower mass, because in these models helium is consumed faster.

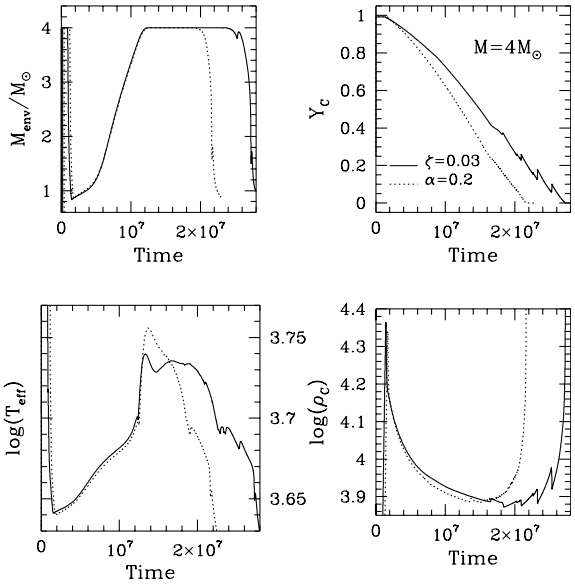

Fig. 9. The comparison between the evolutions of two models of 4 $M_{\odot}$ calculated with a diffusive (solid) and an instantaneous (dotted) scheme for chemical mixing. The four panels show the variation with the He-burning time of the base of the outer convective zone (*left-upper panel*), the central helium mass-fraction (*right-upper panel*), the effective temperature (*left-bottom*) and the central density (*right-bottom*).

4.1. The nuclear and mixing time-scales

From the above discussion it is evident that the reason for the diffusive scheme leading to slightly longer He-burning times and to generally longer fraction of time spent in the blue region of the clump is readily explained by a slower helium consumption in comparison with the instantaneous case. As can be seen in the bottom panel of Fig. 8, this difference is particularly relevant for the 4 $M_{\odot}$ model, so we temporarily focus our attention on this mass. Qualitatively, we expect the same arguments to hold even for slightly larger masses.

In the four panels of Fig. 9 we compare the temporal evolution of some chemical and physical quantities related to the evolution of the two models. The small irregularities present in the diffusive model (solid track) have been widely discussed in Sect. 3.1. Here we only note that in the instantaneous model (dotted track) such discontinuities in the temporal evolution of the various physical and chemical quantities are practically absent, because the small convective zone which forms next to the formal border of central convection (see Sect. 3.1) is well inside the overshooting zone (whose width is $0.2H_{\rm p}$), which is fully mixed in the instantaneous scheme.

In both cases we see that the surface convection is extinguished ≈12 Myr after the beginning of helium burning (left-upper panel). An analogous behaviour of the helium burning does not correspond to this similarity between the times of the recession of the convective envelope: in the right-upper panel we see that helium consumption is faster in the instantaneous model (dotted track), so that, when the bluest point is reached, the central mass fraction of helium is $Y_{\rm C} = 0.65$ in the diffusive case, while it is only $Y_{\rm C} = 0.4$ in the instantaneous model. As already pointed out in the previous section, this lower helium abundance determines an earlier start of the core-contraction, and a quick return of the track to the red (see the bottom panels).

To resolve all doubts related to a possible occurrence of any difference arising from the physical and chemical structure of the models at the beginning of the He-burning phase, we calculated four evolutionary sequences beginning from the same starting model, at the tip of the giant branch, adopting a diffusive scheme for mixing with parameters $\zeta = 0.02$ and $\zeta = 0.03$, and an instantaneous mixing approximation with overshooting parameters $\alpha = 0.2$ and $\alpha = 0.3$. The evolution from the pre-MS phase up to the beginning of He-burning was calculated with $\zeta = 0.03$.

In the three panels of Fig. 10 we compare the four evolutions. We see that in all the sequences the rapidity with which the surface convection recedes (top panel) and the CNO burning shell moves outwards (middle panel) is the same, while in the instantaneous models helium is burning faster: what is interesting is that this qualitative difference between the two sets of models holds independently of the values of the free parameters α and ζ, and seems to be more related to the details of the mixing scheme adopted. All the models show the same evolution for the outer layers of the star, starting from the CNO

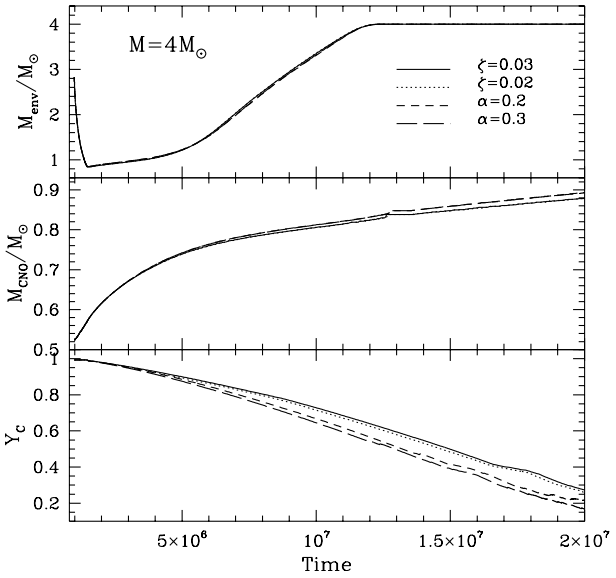

Fig. 10. The evolution from the tip of the giant branch of four 4 $M_\odot$ models calculated from the same starter file. The solid and dotted lines refer to diffusive models differing in the ζ coefficient, while the dashed and the dashed-dotted lines indicate the evolutions of two instantaneous models. The three panels report the variation of the mass of the base of the envelope (*top*), the mass where the peak of the CNO burning shell is located (*middle*) and the central mass fraction of helium.

burning shell, but the evolutions of the core vary with the mixing scheme.

We stress that these differences are more relevant here than in the context of H-burning, because in this latter case we know that the core shrinks in mass as H-burning proceeds, and this tends to level any difference.

A deeper inspection of the physical situation in the interior of the core may help in understanding the differences in the He-burning among the models. As already shown in Fig. 5, the 4 $M_\odot$ model develops a convective core (we refer only to the formal convective region, excluding for the moment any extra-mixing zone) whose extension in mass stabilises to $M_C \approx 0.29\ M_\odot$ shortly after the beginning of He-burning. Within this region the efficiency of convection is so high (due to the high densities) that the temperature gradient is practically adiabatic. The average velocity of the convective eddies reaches a maximum value of $v_{max} \approx 100$ m s^{-1} in the proximity of the centre of the star, and then declines to $v_b \approx 10$ m s^{-1} at points where the formal border of the core is located (see Fig. 7). These velocities lead to a typical time of mixing of the order of $\tau_{mix} \approx 2$ days in most parts of the core, which is extremely short compared to the time scale of nuclear burning by the 3α and by the $^{12}C + \alpha$ reactions, which are of the order of $\tau_{nucl} \approx 10^5$ yr in the centre, and $\tau_{nucl} \approx 10^{10}$ yr at the Schwarzschild border (actually, the He-burning time gets progressively shorter as He-burning proceeds due to the increase of the temperature, but the variations are at most by a factor of ten, and do not change our main conclusions). This discussion confirms that in the whole region which is unstable to convective motions the use of the instantaneous mixing approximation is consistent with its basic assumption, i.e. convection is so fast with respect to the nuclear processes that the whole region is instantaneously homogenised.

The inclusion of overshooting has the effect of increasing the size of the convective core: a distance of $l_{ov} = 0.2H_p$ makes the extension in mass of the core to increase by $\delta M \approx 0.04\ M_\odot$, and $l_{ov} = 0.3H_p$ corresponds to $\delta M \approx 0.08\ M_\odot$. In this extra-mixing regions the velocities decrease to a few m s^{-1}, so that the times scale of convection increase, up to $\tau_{mix} \approx 10^5$ yr. Hence, in these regions the rapidity with which convection tends to homogenise the structure is comparable to the velocity with which helium is burnt in the central layers, so that the instantaneous mixing approximation does not hold. In this case, if the diffusive approach is used, further helium from the outer layers of the star is still added to the central regions, but this takes a longer time when compared to the instantaneous scheme, so that the helium burning process takes longer. The extension of the extra-mixing region where the instantaneous mixing approximation still holds depends on the details of the velocity decay from the border, hence on the value of ζ that is used, but, with the exception of extremely low values of ζ, there will be in any case a region which is assumed to be fully homogenised in the instantaneous case, which is mixed on longer time-scales in the diffusive approach. This is the ultimate reason for the different qualitative behaviour of the instantaneous and the diffusive models that can be seen in Fig. 10.

The same qualitative arguments still hold if we consider larger masses. In the 8 $M_\odot$ modes, for example, the slightly different thermodynamic conditions of the core favour convective velocities that are larger by a factor of ≈2 with respect to the 4 $M_\odot$ case, but the larger extension of the core makes the mixing time scales very similar in the two cases. The higher temperatures in the 8 $M_\odot$ case make the nuclear time scale shorter, but the difference is contained within one order of magnitude. Therefore, even in this case we expect the presence of a region out of the convective border that is only partly mixed in the diffusive case, which makes the whole He-burning phase longer. This is confirmed by looking at Fig. 11, where we can see the two 8 $M_\odot$ calculated with the diffusive (solid track) and the instantaneous (dotted line) scheme for mixing differ in the He-burning times, the instantaneous model being faster. Unlike the 4 $M_\odot$ model we note from Fig. 11 that in this case also the times for the recession of the convective envelope are different, so that at the beginning of the excursion of the track to the blue the two models have approximately the same amount of helium left in the core: this acts in favour of a similar fraction of time spent in the blue part of the HR diagram during He-burning, and is the reason why the gap between the ratio of the time spent in the blue and red part of the clump decrease with mass.

We may conclude that, if we are interested in a correct estimate of the He-burning time of IMS, and particularly in the relative duration of the blue and the red phase, the use of the diffusive scheme for chemical mixing is recommended for models with mass $M \leq 6\ M_\odot$. The instantaneous mixing scheme would underestimate the total He-burning time, and the duration of the stay of the track in the blue region of the clump. Only for more massive models does the instantaneous mixing scheme lead to results similar to those found by using the diffusive approach.

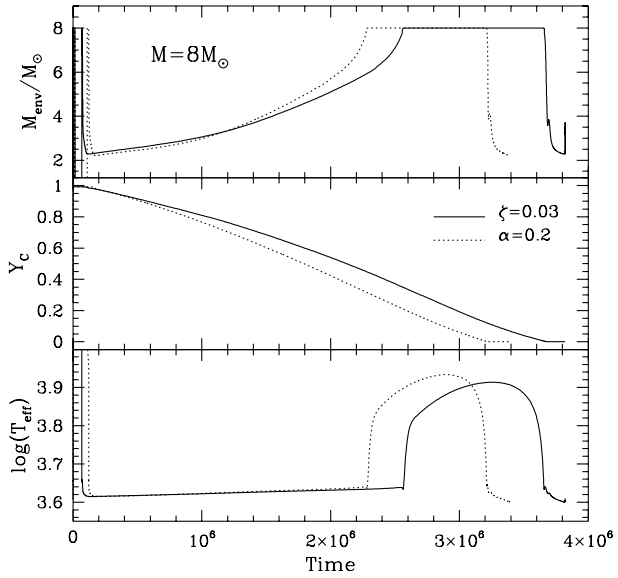

Fig. 11. The comparison between the evolutions of two 8 $M_{\odot}$ models calculated with a diffusive (solid line) and an instantaneous scheme (dotted) for chemical mixing inside the convective core. The three panels show the variation with time of the mass at which the base of the external envelope is located (*top*), the central helium mass fraction (*middle*) and the effective temperature (*bottom*).

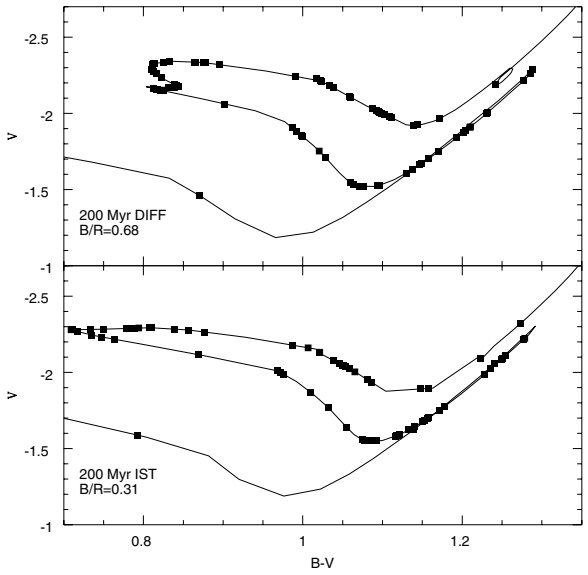

Fig. 12. The solid tracks in the two panels represents the theoretical isochrones corresponding to an age of 200 Myr calculated with a diffusive (*top*) and an instantaneous (*bottom*) scheme for chemical mixing. The squares superimposed on the isochrones are the results of our numerical simulations.

4.2. The clump population of open clusters

The discussion of the previous subsection shows that a particular range of stellar masses exists for which the relative duration of the red and blue phase of He-burning show a dependency on the scheme used to deal with mixing and burning in the central core.

To understand in which cases the description of mixing in the central regions is relevant for the theoretical interpretation

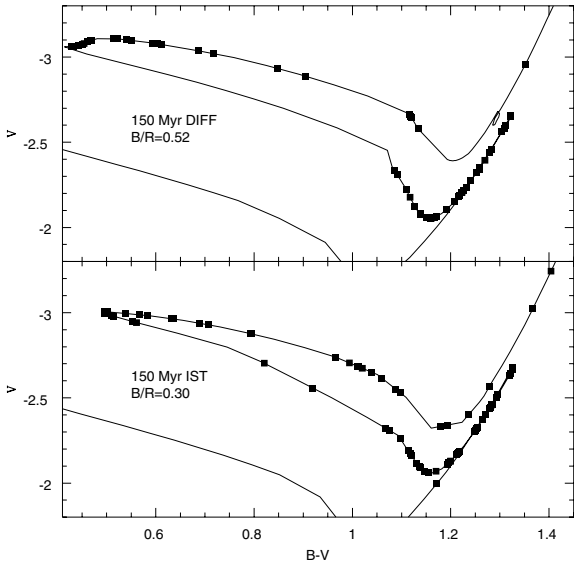

Fig. 13. The same as Fig. 12, but for an age of 150 Myr.

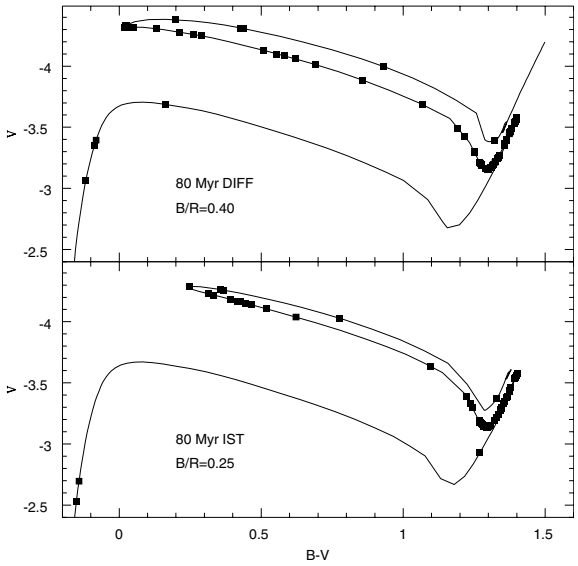

Fig. 14. The same as Fig. 12, but for an age of 80 Myr.

of observational photometric results we constructed isochrones for the instantaneous and the diffusive models corresponding to ages in the range 50−250 Myr both in the theoretical and in the observational plane. We ruled out older ages because in those cases the extension of the clump, in terms of the excursion of the track to the blue, is very short, rendering it extremely difficult to identify a red and a blue region (see the track of the 3 $M_{\odot}$ model in Fig. 1). To construct the isochrones we followed the scheme suggested by Pols et al. (1998); the transformations from the theoretical to the observational plane, for those concerning the $B-V$ colours and the bolometric corrections, were performed by using the tables by Castelli et al. (1997). For each isochrone we performed a numerical simulation on the observational plane.

Such numerical simulations were built following the procedure already described in VC05, that we briefly recall in the following. First, each selected isochrone was populated with a

random distribution of masses; then, for each extracted mass, we obtained by linear interpolation the corresponding values of Log L and Log T_e, as well as magnitudes and colours in the observational plane. Once we populated a given isochrone, we were able to derive the B/R value, by simply counting the number of stars that fall within *appropriate boxes* (see below) in the CM diagram.

To obtain a reliable estimate of B/R, we carefully selected different boxes for isochrones of different ages, taking into account, in particular, the specific magnitude and colour extension of the "blue loop". We decided not to overlap "blue" and "red" boxes, in order to make our statistics more robust against small fluctuations in colour. To provide an estimate of the statistical fluctuation related to the random extraction of star masses, we performed ten simulations for each age, varying only the seed for random number generation, thereby deriving the mean B/R and the corresponding standard deviation for each set of simulations (in this context, small values of standard deviations can be regarded as an indication of the goodness of our choice of the specific shape of blue and red boxes).

We show three of such simulations in Figs. 12–14. We focus our attention on the region of the clump; for clarity all the stars in the H-burning phase were omitted from the figures. For the performed statistical analysis to be relevant, we supposed that the clump contains a considerable large number of stars (≈50), as is the case, for example, for NGC1866 (Testa et al. 1999). In all cases we see that it is possible to identify two distinct regions in the diagram where He-burning takes place: the excursion of the track to the blue, and the return to the red, are very quick, rendering extremely small the probability of finding stars there.

As expected on the basis of the previous discussions, the differences between the predictions of the two sets of models are more relevant for the ages at which the typical mass of the He-burning stars is $M \approx 4\ M_\odot$ (see the bottom panel of Fig. 8), i.e. 200 Myr; we see from Fig. 12 that the B/R ratio is ≈0.7 for the diffusive case, and is only ≈0.3 for the instantaneous models. These differences diminish for younger ages (hence, larger clump masses): for $t = 150$ Myr (see Fig. 13), for which the typical mass of the stars in the clump is $M \approx 4.5\ M_\odot$, the instantaneous B/R is the same as before, i.e. ≈30%, while the diffusive value drops to ≈50%;

For younger ages the mass of the stars involved shifts into the range of values for which, independently of the details of the scheme followed to couple mixing and nuclear burning, the duration of the track in the blue is shortened by the scarcity of helium in the central regions: the simulation shown in Fig. 14, which refers to an age of 80 Myr (and to a mass of the clump of $\approx 6\ M_\odot$) demonstrates that the gap between the results of the two schemes reduces further, the predicted B/R ratios being ≈40% and ≈25%, respectively, for the diffusive and the instantaneous models; our numerical simulations performed for younger ages show that the differences between the predictions concerning the B/R ratio for the two classes of models become too low to be statistically relevant.

Therefore for a metallicity typical of the LMC, the use of a diffusive approach, when compared to the instantaneous case, leads to a prediction of a larger population of He-burning stars in the blue part of the region of the clump, but these differences are limited to ages in the range 80−200 Myr, for which the typical masses in the He-burning phase are $4\ M_\odot \leq M \leq 6\ M_\odot$; for older ages the extension of the clump itself is so short that it does not allow one to identify two distinct regions, while for younger ages the differences between the predictions of the two sets of models are not statistically relevant.

5. Conclusions

We present detailed evolutionary models that focus on the core hydrogen- and helium-burning phases of intermediate mass stars, with masses up to $M = 9\ M_\odot$; the present investigation employs a metallicity typical of the LMC, i.e. $Z = 0.008$.

We carefully compare the results obtained with the traditional instantaneous mixing approximation when applied to chemical mixing and nuclear burning in the convective core, and those found by treating the two mentioned processes simultaneously, in a self-consistent way, with a diffusive approach.

During the H-burning phase no relevant differences are found in the results between the two schemes for mixing, because the convective core of these stars tends to shrink in mass; given a value of the mass of the star, the duration of this phase is almost independent of the mechanism chosen to deal with mixing.

In contrast to the H-burning phase, we find different results during the later phase of He-burning when the diffusive scheme is used. Helium from the outer layers, in the proximity of the formal core defined by the Schwarzschild criterion, is similarly efficient but more slowly mixed into the central regions in comparison to the instantaneous models, and this leads to two important differences:

1. For a given mass, the duration of the entire He-burning phase, and consequently the t(He)/t(H) ratio, is longer in the diffusive models.
2. In the diffusive models the fraction of the time spent in the blue region of the clump is larger than in the corresponding instantaneous models; this is the consequence of the more rapid helium consumption in the instantaneous case, which, as soon as the track reaches the bluest point in the HR diagram, favours an early contraction of the core and a return of the track to the red.

Both above effects are particularly relevant for models with mass $M \leq 6\ M_\odot$, because for higher masses the larger mass of the envelope (which triggers a later exhaustion of surface convection) and the more rapid burning of helium forces the track to return quickly to the red. Therefore, in the interpretation of the stellar population of open clusters, the differences introduced by the use of the diffusive approach are relevant for stellar models in the range $3.5\ M_\odot \leq M \leq 6\ M_\odot$, and for ages in the range 80 Myr $\leq t \leq$ 200 Myr.

These results prove to hold independently of all the uncertainties that characterise the choice of the diffusion coefficient entering into the diffusion equation, which ultimately depends on the velocity profile within and out of the central region: in the proximity of the core the values of the velocities found via

the local FST model for turbulent convection turned out to be very similar to those obtained via a non-local theory, and this holds independently of all the free parameters entering both treatments. The differences between the diffusive and the instantaneous models in the afore-mentioned range of masses is essentially related to the way with which helium is mixed from the outer layers into the central regions, which is governed by an exponential decay of convective velocities. The choice of parameters (e.g. the assumed distance of the exponential decay or the extension of the overshooting region in the instantaneous models) associated with a selected mixing scheme turns out to be largely insignificant.

References

Alongi, M., Bertelli, G., Bressan, A., et al. 1993, A&AS, 97, 851
Angulo, C., Arnould, M., Rayet, M., et al. 1999, Nucl. Phys. A, 656, 3
Barmina, R., Girardi, L., & Chiosi, C. 2002, A&A, 385, 847
Böhm-Vitense, E. 1958, Z. Astroph., 46, 108
Bressan, A., Bertelli, G., & Chiosi, C. 1981, A&A, 102, 25
Brocato, E., Castellani, V., Di Carlo, E., Raimondo, G., & Walker, A. R. 2003, AJ, 125, 3111
Canuto, V. M., Goldman, I., & Mazzitelli, I. 1996, ApJ, 473, 570
Canuto, V. M., & Mazzitelli, I. 1991, ApJ, 370, 295
Canuto, V. M. 1997, ApJ, 489, L71
Castellani, V., Chieffi, A., Pulone, L., & Tornambè, A. 1985a, ApJ, 296, 204
Castellani, V., Giannone, P., & Renzini, A. 1971a, Astr. Space Sci., 10, 340
Castellani, V., Giannone, P., & Renzini, A. 1971b, Astr. Space Sci., 10, 355
Castelli, F., Gratton, R. G., & Kurucz, R. L. 1997, A&A, 324, 432
Caughlan, G. R., & Fowler, W. A. 1988, Atom. Data Nucl. Tab., 40, 283
Chiosi, C., Bertelli, G., & Bressan, A. 1992, ARA&A, 30, 235
Cloutman, L., & Eoll, J. G. 1976, ApJ, 206, 548
Cottrell, P. L., & Da Costa, G. S. 1981, ApJ, 245, 79
D'Antona, F. 2002, in Extragalactic Star Clusters, ed. D. Geisler, E. K. Grebel, & D. Minniti, IAU Symp. Ser., 207
D'Antona, F., Gratton, R., & Chieffi, A. 1983, Mem. S.A.It., 54, 173
Demarque, P., Sarajedini, A., & Guo, X.-J. 1994, ApJ, 426, 165
Deng, L., Bressan, A., & Chiosi, C. 1996a, A&A, 313, 145
Deng, L., Bressan, A., & Chiosi, C. 1996b, A&A, 313, 159
Freytag, B., Ludwig, H. G., & Steffen, M. 1996, A&A, 313, 497
Gratton, R., Sneden, C., & Carretta, E. 2004, ARA&A, 42, 385
Grossman, S. A. 1996, MNRAS, 279, 305
Iben, I. J. 1975, ApJ, 196, 525
Iben, I. J. 1976, ApJ, 208, 165
Iben, I. J. 1993, ApJ, 415, 767
Kunz, R., Fey, M., Jaeger, M., Mayer, A., & Hammer, J. W. 2002, ApJ, 567, 643
Kuhfuß, R. 1986, A&A, 160, 116
Maeder, A., & Mermilliod, J. C. 1981, A&A, 93, 136
Maeder, A., & Meyner, G. 1991, A&AS, 89, 451
Mazzitelli, I., D'Antona, F., & Ventura, P. 1999, A&A, 348, 846
Pietrinferni, A., Cassisi, S., Salaris, M., & Castelli, F. 2004, ApJ, 612, 168
Pols, O. R., Schroder, K. P., Hurley, J. R., Tout, C. A., & Eggleton, P. P. 1998, MNRAS, 298, 505
Prather, M. J., & Demarque, P. 1974, ApJ, 193, 109
Salasnich, B., Bressan, A., & Chiosi, C. 1999, A&A, 342, 131
Schmidt, E. G. 1984, ApJ, 356, 915
Schwarzschild, M., & Härm, R. 1965, ApJ, 142, 855
Schwarzschild, M., & Härm, R. 1967, A&A, 145, 486
Stancliffe, R. J., Tout, C. A., & Pols, O. R. 2004, MNRAS, 352, 984
Stellingwerf, R. F. 1982, ApJ, 262, 339
Stellingwerf, R. F. 1984, ApJ, 284, 712
Stothers, R. B., & Chin, C. W. 1992, ApJ, 390, 136
Stothers, R. B., & Chin, C. W. 1995, ApJ, 440, 297
Stothers, R. B., & Chin, C. W. 1997, ApJ, 478, L103
Testa, V., Ferraro, F., Chieffi, A., et al. 1999, AJ, 118, 2839
Ventura, P., & Castellani, M. 2005, A&A, 430, 1035
Ventura, P., & D'Antona, F. 2005, A&A, 431, 279
Ventura, P., D'Antona, F., & Mazzitelli, I. 2002, A&A, 393, 215
Ventura, P., D'Antona, F., Mazzitelli, I., & Gratton, R. 2001, ApJ, 550, L65
Ventura, P., Zeppieri, A., D'Antona, F., & Mazzitelli, I. 1998, A&A, 334, 953
Vitense, E. 1953, Zs. Ap., 32, 135
Xiong, D. R. 1981, Scient. Sin. XXIV., 10, 1406
Xiong, D. R. 1985, A&A, 150, 133
Zahn, J.-P. 1991, A&A, 252, 179